Observation and Modeling of Interrupted Pattern Coarsening: Surface Nanostructuring by Ion Erosion

Javier Muñoz-García,[1] Raúl Gago,[2] Luis Vázquez,[2] José Angel Sánchez-García,[2] and Rodolfo Cuerno[3]
[1]*Systems Biology Ireland and Grupo Interdisciplinar de Sistemas Complejos (GISC), University College Dublin, Belfield, Dublin 4, Ireland*
[2]*Instituto de Ciencia de Materiales de Madrid, Consejo Superior de Investigaciones Científicas, E-28049 Madrid, Spain*
[3]*Departamento de Matemáticas and GISC, Universidad Carlos III de Madrid, E-28911 Leganés, Spain*
(Received 6 November 2009; published 12 January 2010)

We report the experimental observation of interrupted coarsening for surface self-organized nanostructuring by ion erosion. Analysis of the target surface by atomic force microscopy allows us to describe quantitatively this intriguing type of pattern dynamics through a continuum equation put forward in different contexts across a wide range of length scales. The ensuing predictions can thus be consistently extended to other experimental conditions in our system. Our results illustrate the occurrence of nonequilibrium systems in which pattern formation, coarsening, and kinetic roughening appear, each of these behaviors being associated with its own spatiotemporal range.

DOI: 10.1103/PhysRevLett.104.026101 PACS numbers: 68.35.Ct, 05.45.−a, 79.20.Rf, 81.16.Rf

Morphology formation and dynamics rank among the most fascinating topics within nonequilibrium phenomena on spatially extended systems. They encompass from emergence of well defined, ordered patterns [1] to scale invariant, disordered behavior (kinetic roughening) [2], large-scale properties being often independent of specific details of the preparation techniques and of the materials employed (*universality*). A third conspicuous realm of universality is that of *coarsening* phenomena [3], whereby the characteristic feature size of a pattern ℓ evolves nontrivially with time t. Coarsening occurs in very diverse systems, from colloids [4] to social dynamics [5], to ion-beam erosion of solid targets [6,7]. Actually, an open question in pattern formation at large concerns identifying general criteria [8] to predict the type of evolution of ℓ [9], ranging from remaining a constant, to power-law behavior, interrupted coarsening (IC), or spatiotemporal chaos. In particular, IC has arisen as a novel type of dynamic behavior whose relevance to, e.g., formation of giant Aeolian sand dunes has been recently invoked [10]. Although in its original formulation IC refers to a pattern that stops growing in ''lateral'' size (ℓ) while perpetually increasing in ''vertical'' size (amplitude), more recently other systems have been identified in which an analogous interruption of wavelength *and* amplitude occur, yielding to kinetic roughening at the largest time and length scales [11,12]. Models with this behavior have been derived for diverse contexts and scales, from amorphous thin film growth [13] to ion-beam nanostructuring [14,15], to patterns on snow fields [16], and belong to a class that remains to date as a theoretical challenge in the identification of the various coarsening scenarios.

In this Letter we report the experimental observation of IC, for the case of surface nanopattern formation by ion-beam sputtering (IBS) of silicon targets. This validates the physical relevance of the IC scenario, in particular, in the form that it takes for cases as in [11–16]. Specifically, our morphological observations are contrasted with the theoretical approximations given in [12], allowing for a full quantitative description of the experimental dynamics through the continuum model proposed in this reference, to the extent that the pattern behavior can also be accounted for when experimental parameters are changed. As a side result, our theoretical description allows us to identify the nature of the main surface smoothing mechanism in the experiments to be ion-induced, a conclusion of interest on its own right.

We thus focus on self-organized nanopattern formation by IBS, that has attracted recent interest as a *bottom-up* nanostructuring technique due to its applicability to metal, semiconductor, and insulator surfaces. Moreover, it provides an example of nonequilibrium systems where a rich variety of pattern formation processes (nanoripples, nanodots, etc.) is indeed found [6,17]. Si targets (380 μm thick, p type, 1–10 Ω cm) were sputtered with 1 keV Ar^+ ions at normal incidence. The ions were extracted from a commercial 3 cm beam-diameter CSC Kaufman-type ion gun (VEECO). The sample current density was adjusted prior to the process with a Faraday Cup located on a movable shutter covering the target. The values obtained were further checked by calibration of the erosion rate, as derived from the etched depth by profilometry. For this purpose, the step created between the exposed and the masked parts of the sample was measured with a Dektak 150 mechanical profiler (VEECO). This masking procedure introduces metal (Fe) impurities during the IBS process, which could influence the pattern morphology. For example, nanohole morphologies are induced instead of nanodot pattern when the residual metal content on the target surface is high [18]. In our case, these Fe impurities are incorporated systematically in all samples and within the same range ($1–2 \times 10^{15}$ at/cm^2), as assessed by Rutherford backscattering

spectrometry, and only dot patterns are induced. Irradiations were performed with no intentional sample heating, checking that the target temperature was not above 200 °C due to ion impingement. The resulting surface topography was imaged by atomic force microscopy (AFM) with a Nanoscope IIIa (VEECO) equipment operating in tapping mode in air and using silicon cantilevers.

Figures 1(a)–1(c) show the AFM images of irradiated Si surfaces at different times for the ion flux $\Phi_1 = 6 \times 10^{14}$ ions cm^{-2} s^{-1}. The obtained morphologies are similar to those previously reported [19]. The AFM data shows the formation of nanodot patterns with short-range in-plane hexagonal order as observed from the height autocorrelation function displayed as insets in Figs. 1(a)–1(c). The definition of the hexagonal arrangement in the correlation functions reveals in-plane order enhancement with sputtering time. This trend has been previously observed in single-element and compound semiconductors [6,17]. The power spectral density (PSD) of the AFM images allows us to obtain the basic pattern wavelength ℓ related to the finite peak of the PSD curve ($\ell = 2\pi/k$). In Fig. 1(d) we can observe a shift of the PSD peak towards small k values indicating pattern coarsening. Also, the increase of the intensity of the PSD with time at low k values reflects surface roughening. Figure 2 shows more quantitative analysis of the surface morphology for the present flux value (black triangles). A sharp initial increase of the global surface roughness σ (integral of the PSD over k) is due to the appearance of the peak in the PSD (linear instability), followed by slower growth with time [Fig. 2(a)]. Likewise, coarsening of ℓ is observed [Fig. 2(b)], although it is interrupted for long enough irradiation times, after which both σ and ℓ reach stationary values. Although coarsening has been reported experimentally in ripple formation by IBS [7,20], results remain controversial for nanodot patterns on semiconductor surfaces [21–23].

Classically, pattern formation under IBS has been understood as the interplay between the (unstable) dependence of the sputtering yield on surface curvature and stabilizing surface relaxation mechanisms. Continuum descriptions follow the seminal work by Bradley and Harper (BH) [24], in which an evolution equation is derived for the target height, $h(x, y, t)$, above point (x, y) on a reference plane. The linear BH theory and later extensions [25,14] have provided relevant information about the main operating mechanisms as well as qualitative predictions on properties like the wavelength dependence on some experimental parameters, ripple orientation as a function of the incidence angle, etc. However, description of other important pattern features, such as coarsening and ordering, has required the coupling of h with an additional field related with the density of material subject to surface

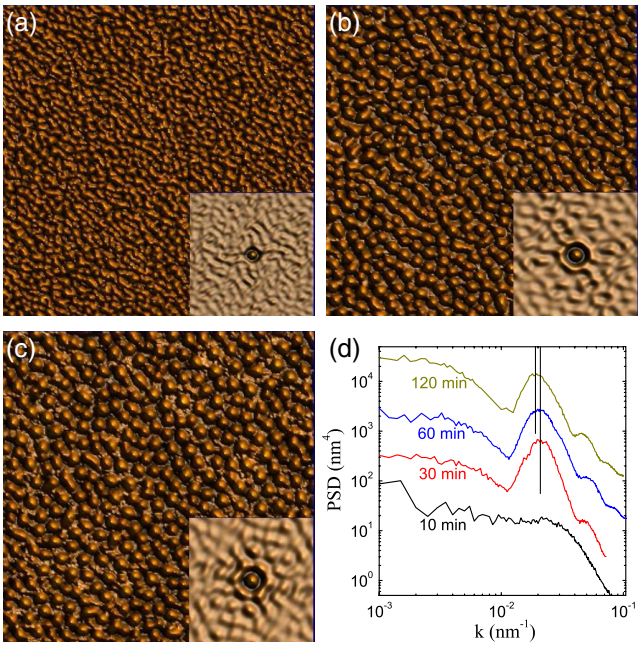

FIG. 1 (color online). AFM 1×1 μm^2 images of the Si surfaces sputtered with 1 keV Ar^+ for $\Phi_1 = 6 \times 10^{14}$ ions cm^{-2} s^{-1} at times: (a) $t = 10$ min, (b) $t = 30$ min, and (c) $t = 60$ min. The insets show the corresponding autocorrelation images taken over a 400×400 nm^2 area. (d) PSD curves extracted from the AFM data at different times. Curves for $t > 10$ min have been shifted vertically for the sake of clarity.

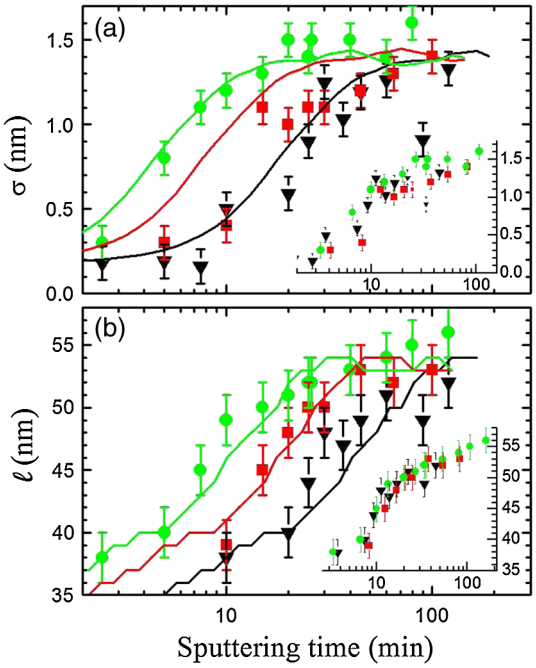

FIG. 2 (color online). (a) Time evolution of the global roughness $\sigma(t)$ and (b) the pattern wavelength $\ell(t)$ for different values of Φ: (black triangles) $\Phi_1 = 6 \times 10^{14}$ ions cm^{-2} s^{-1}, (red squares) $\Phi_2 = 14 \times 10^{14}$ ions cm^{-2} s^{-1}, and (green circles) $\Phi_3 = 25 \times 10^{14}$ ions cm^{-2} s^{-1}, as extracted from AFM data. The solid lines represent the corresponding results from numerical simulations of Eq. (1). The insets show the same experimental data vs the ion fluence (units of x axis are 10^{17} ions cm^{-2}).

transport, akin to descriptions of pattern formation on aeolian sand dunes [26]. In spite of all these efforts, a fully consistent quantitative description the IBS system is still lacking [6,17].

For IBS under normal incidence as in our experiment, the effective evolution equation for the height is [12,15]

$$\frac{\partial h}{\partial t} = -\nu\nabla^2 h - \mathcal{K}\nabla^4 h + \lambda_1(\nabla h)^2 - \lambda_2\nabla^2(\nabla h)^2, \quad (1)$$

where (positive) coefficients ν, $\mathcal{K}$, $\lambda_{1,2}$ depend on phenomenological parameters (flux, ion energy, etc.). Although Eq. (1) has been in principle formulated for single compound materials, the destabilizing effect on which its derivation has been based seems to be enhanced by contamination [17], allowing Eq. (1) to reproduce also the features of some experimental systems in which impurities may be present. Equation (1) shows IC in which an ordered cell (dot) pattern develops initially, that coarsens during a transient time. For later times a pattern remains featuring both constant wavelength and amplitude at intermediate distances, while the profile is disordered and rough at larger distances. Two important limits of Eq. (1) are the $\lambda_2 = 0$ and the $\lambda_1 = 0$ cases. The former is the celebrated Kuramoto-Sivashinsky (KS) equation [27,28], paradigmatic of spatiotemporal chaos, for which a (disordered) short-range pattern develops with a wavelength that does *not* coarsen, kinetic roughening occuring at much larger scales [29]. The $\lambda_1 = 0$ case is the "conserved" KS equation (CKS), appearing, for dynamics of amorphous thin films [13] and steps on vicinal surfaces [30], for which the linear instability leads to an *ordered* pattern of paraboloids with *uninterrupted* coarsening.

For generic parameter values, Eq. (1) interpolates between the KS and CKS limits. Actually, approximate analytical predictions from [12] allow us to estimate the values of the coefficients in Eq. (1) that correspond to our experimental results. Thus, the linear instability wavelength is given by $\ell_l = 2\pi(2\mathcal{K}/\nu)^{1/2}$. An estimation of the time associated with instability onset is given by the inverse value of the linear dispersion relation at maximum, $t_l = 4\mathcal{K}/\nu^2$. Finally, after coarsening the asymptotic pattern wavelength differs from its value at instability onset and is given, rather, by $\ell_f = (32\lambda_2/\lambda_1)^{1/2}$, whereas the stationary dot amplitude $A_f \simeq 1.25\nu/\lambda_1$. All the coefficients in Eq. (1) are strictly proportional to Φ [12]. The exception is $\mathcal{K}$, that measures the effective surface diffusion and reflects, in principle, both thermally activated and ion-beam induced material transport. For our particular conditions ("low" Φ and temperature ranges), we expect the morphological features to be independent of Φ (see below), suggesting that the only diffusion process is ion-induced, in which case $\mathcal{K}$ is also proportional to Φ.

For the above experimental data corresponding to Φ_1, we take $t_l \simeq 6.25$ min, $\ell_l \simeq 35$ nm, $l_f \simeq 50$ nm, and $A_f \simeq 4$ nm, leading to $\nu = 10\ \mathrm{nm}^2/\mathrm{min}$, $\mathcal{K} = 156\ \mathrm{nm}^4/\mathrm{min}$, $\lambda_1 = 3\ \mathrm{nm}/\mathrm{min}$, and $\lambda_2 = 236\ \mathrm{nm}^3/\mathrm{min}$. Using these coefficient values, we have integrated Eq. (1) numerically. The experimental and theoretical profiles for Φ_1 are compared in Figs. 3(a) and 3(b). Statistically, both the amplitude and width of the structures coincide for the same times. Furthermore the height disorder (measured by the global roughness) is also quite similar both at 10 and 30 min. In order to perform a more quantitative comparison for the behavior of σ and ℓ, their time evolution according to Eq. (1) has been plotted in Fig. 2 (black solid lines). The different experimental values of ℓ_l and ℓ_f are thus seen to conform to the description by a (simplified) continuum model. However, slight differences remain between the analytical estimates for ℓ_f and A_f [12], and their values as obtained from the numerical integration of Eq. (1). These discrepancies can be justified noting that the predictions for the final dot amplitude and wavelength are valid for substantial coarsening processes, i.e., provided $\ell_l \ll \ell_f$. Using the expressions for ℓ_l and ℓ_f, this amounts to requiring $r \equiv \nu\lambda_2/(\mathcal{K}\lambda_1) \gg \pi^2/4$. Note, the nondimensional parameter r measures [11,12] the degree of interpolation between the KS ($r = 0$) and CKS ($r = \infty$) limits. For our experiments $r \simeq 5$, near the validity limit for the analytical estimates.

As a further check, we consider the application of Eq. (1) to different experimental conditions. Assuming as mentioned above that all coefficients in Eq. (1) are proportional to Φ, it is now straightforward to obtain their values for different flux conditions. Thus, for $\Phi_2 = 14 \times 10^{14}\ \mathrm{ions\,cm^{-2}\,s^{-1}}$ and $\Phi_3 = 25 \times 10^{14}\ \mathrm{ions\,cm^{-2}\,s^{-1}}$ we obtain, respectively, $\nu = 23\ \mathrm{nm}^2/\mathrm{min}$, $\mathcal{K} = 364\ \mathrm{nm}^4/\mathrm{min}$, $\lambda_1 = 7\ \mathrm{nm}/\mathrm{min}$, $\lambda_2 = 550\ \mathrm{nm}^3/\mathrm{min}$, and $\nu = 42\ \mathrm{nm}^2/\mathrm{min}$, $\mathcal{K} = 650\ \mathrm{nm}^4/\mathrm{min}$, $\lambda_1 = 12.5\ \mathrm{nm}/\mathrm{min}$, $\lambda_2 = 982\ \mathrm{nm}^3/\mathrm{min}$. Since we are multiplying all the coefficients in Eq. (1) by a proportionality constant, the effect is merely a rescaling of time. The time

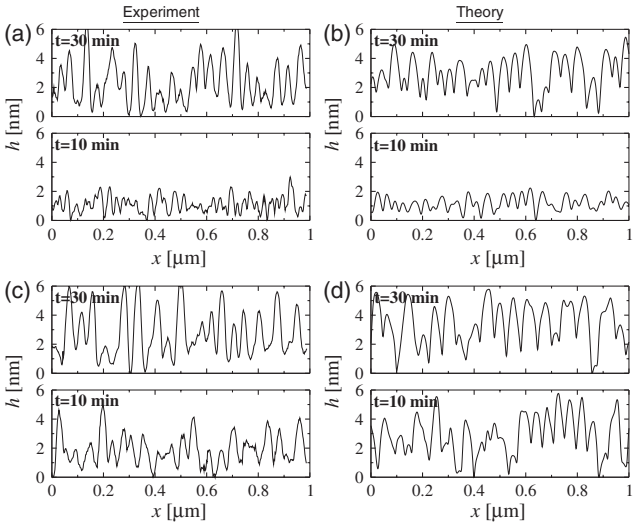

FIG. 3. Experimental AFM (left) and numerical (right) longitudinal profiles for (a),(b) $\Phi_1 = 6 \times 10^{14}\ \mathrm{ions\,cm^{-2}\,s^{-1}}$ and (c), (d) $\Phi_3 = 25 \times 10^{14}\ \mathrm{ions\,cm^{-2}\,s^{-1}}$ after 10 and 30 min.

evolutions of σ and ℓ for these new coefficient values are plotted in Fig. 2, in which the experimental data for Φ_2 and Φ_3 are also shown. Again, the quantitative agreement between the experimental and the analytical results is remarkable for all times [compare also Figs. 3(c) and 3(d)]. The pattern onset and stabilization take place earlier at higher Φ values and present similar features after prolonged irradiation. The insets of Fig. 2 show the experimental evolution of σ and ℓ as a function of the ion fluence or dose (flux multiplied by irradiation time). As predicted, the collapse of the plots indicates that the pattern characteristics are only determined by the total number of ions that impinged onto the surface, and corroborates that the main mechanism for surface relaxation in the present experiments is ion-induced diffusion. Moreover, both for the experimental and numerical morphologies the height corrugation appears earlier for higher Φ values. This is also reflected in the PSD curves where the power-law regime at low-k values is broader for the sample bombarded at high flux values (Φ_3) confirming its faster dynamics. The result that the asymptotic morphologies are not affected by the dynamics contrasts with the trend obtained in [31], where a higher erosion rate and a thermal relaxation mechanism led to slightly smaller ℓ_f values and a less defined pattern order for different crystallographic orientations. The observed discrepancy may be explained taking into account the different target temperature reached during irradiation. In particular, from the measurement of the etched depth after irradiation, it is noted that the estimated flux employed in [31] was nearly 3 times the maximum value used here, which might have raised the target temperature enhancing thermally activated surface diffusion.

In summary, for the specific case of IBS nanostructuring, we have been able to describe the full dynamics of an experiment by a single continuum equation. In the quest to improve our theoretical understanding of IBS, this adds to the plausibility of Eq. (1) as a long distance description of the dynamics for many of these systems. Additionally, our experiments have allowed us to establish the nature of the main smoothening mechanism under the present conditions, improving control on final pattern features via experimental conditions.

From a general viewpoint, we have assessed the IC scenario in detail for an experimental system, its dynamics being quantitatively described by the continuum model (1). Agreement between theory and experiment includes the general analytical conditions for the coarsening process to occur and the values of the stationary pattern amplitude and wavelength as compared with values at onset of the linear instability. This underscores the physical relevance of the present type of IC, and the interest of the nonlinear Eq. (1) as an universal model for nonequilibrium systems in which pattern formation, coarsening and kinetic roughening occur, each of them being associated with its own spatiotemporal range.

We are indebted to M. Castro for fruitful suggestions and discussions. This work has been supported by Grant Nos. CSD2008-0023, CSD2007-00010, and FIS2009-12964-C05-01, -04 (MICINN, Spain), and CCG08-CSIC/MAT-3457 (CAM, Spain).

[1] M. Cross and H. Greenside, *Pattern Formation and Dynamics in Nonequilibrium Systems* (Cambridge University Press, Cambridge, England, 2009).
[2] A.-L. Barabási and H. E. Stanley, *Fractal Concepts in Surface Growth* (Cambridge University Press, Cambridge, England, 1995).
[3] A. J. Bray, Adv. Phys. **43**, 357 (1994).
[4] K. Stratford *et al.*, Science **309**, 2198 (2005).
[5] C. Castellano *et al.*, Rev. Mod. Phys. **81**, 591 (2009).
[6] J. Muñoz-García *et al.*, in *Towards Functional Nanomaterials*, edited by Z. M. Wang (Springer, New York, 2009).
[7] H. Hansen *et al.*, Phys. Rev. Lett. **102**, 146103 (2009).
[8] P. Politi and C. Misbah, Phys. Rev. Lett. **92**, 090601 (2004); Phys. Rev. E **73**, 036133 (2006).
[9] We assume arbitrarily long wavelengths to be unstable, as e.g., for surfaces with no preferred height value.
[10] B. Andreotti *et al.*, Nature (London) **457**, 1120 (2009).
[11] J. Muñoz-García, R. Cuerno, and M. Castro, Phys. Rev. E **74**, 050103(R) (2006).
[12] J. Muñoz-García, R. Cuerno, and M. Castro, J. Phys. Condens. Matter **21**, 224020 (2009).
[13] M. Raible, S. J. Linz, and P. Hänggi, Phys. Rev. E **62**, 1691 (2000).
[14] T. C. Kim *et al.*, Phys. Rev. Lett. **92**, 246104 (2004).
[15] M. Castro *et al.*, Phys. Rev. Lett. **94**, 016102 (2005).
[16] T. Tiedje *et al.*, J. Geophys. Res. **111**, F02 015 (2006).
[17] See R. Cuerno *et al.*, J. Phys. Condens. Matter **21**, 220301 (2009), and other papers in the same issue.
[18] J. A. Sánchez-García *et al.*, Nanotechnology **19**, 355306 (2008); J. Phys. Condens. Matter **21**, 224009 (2009).
[19] R. Gago *et al.*, Appl. Phys. Lett. **78**, 3316 (2001); Nanotechnology **13**, 304 (2002).
[20] S. Habenicht and K. P. Lieb, Phys. Rev. B **65**, 115327 (2002).
[21] T. Bobek *et al.*, Phys. Rev. B **68**, 085324 (2003).
[22] M. Xu and C. Teichert, J. Appl. Phys. **96**, 2244 (2004).
[23] S. K. Tan and A. T. S. Wee, J. Vac. Sci. Technol. B **24**, 1444 (2006).
[24] R. M. Bradley and J. M. E. Harper, J. Vac. Sci. Technol. A **6**, 2390 (1988).
[25] R. Cuerno and A.-L. Barabási, Phys. Rev. Lett. **74**, 4746 (1995); M. Makeev, R. Cuerno, and A.-L. Barabási, Nucl. Instrum. Methods Phys. Res., Sect. B **197**, 185 (2002).
[26] Z. Csahók *et al.*, Eur. Phys. J. E **3**, 71 (2000).
[27] G. I. Sivashinsky, Annu. Rev. Fluid Mech. **15**, 179 (1983).
[28] Y. Kuramoto, *Chemical Oscillation, Waves and Turbulence* (Springer, Berlin, 1984).
[29] K. Sneppen *et al.*, Phys. Rev. A **46**, R7351 (1992).
[30] T. Frisch and A. Verga, Phys. Rev. Lett. **96**, 166104 (2006).
[31] R. Gago *et al.*, Appl. Phys. Lett. **89**, 233101 (2006).